DIFFRACTION IN DIS AT HERA

B. LÖHR

Deutsches Elektronen Synchrotron (DESY)
(Notkestrasse 85, 22607 Hamburg, Germany)

UDC 621.1
©2003

In this paper, results are presented from the experiments H1 and ZEUS at HERA on diffractive reactions in photoproduction and in deep inelastic scattering. Data are shown for exclusive vector-meson production, inclusive diffractive scattering, and on deeply virtual Compton scattering (DVCS). The data are compared to Regge phenomenology and the Pomeron trajectories are extracted for the different reactions, except DVCS. Also fits and predictions of perturbative QCD models are compared to the experimental results. From the description of the data in these two approaches it is demonstrated that there is a transition from soft diffraction to hard diffraction when either the mass of the diffractively produced system gets high or the negative four-momentum transfer squared, Q^2, from the electron/positron to the diffractively produced system or the absolute value of the four-momentum transfer squared,$\mid t \mid$, from the proton to the diffractively produced system become large.

1. Kinematics of Deep Inelastic Scattering and Diffractive Scattering

HERA is an electron-proton collider in Hamburg [1]. Electrons or positrons of 27.5 GeV are scattered on protons of 920 GeV. The center of mass energy is $\sqrt{(s)}=$ 318 GeV. In a fixed proton target situation, this is equivalent to an electron energy of 50600 GeV.

In electron-proton scattering, we are dealing with the process which is sketched in Fig. 1. At a fixed center of mass energy, the kinematics of the inclusive process is described by the energy and the angle of the scattered electron. In deep inelastic scattering, the following variables, which are Lorentz invariant, are commonly used instead:

$s = (k + p)^2$: center of mass energy squared of the e-p system,

$Q^2 = -q^2 = -(k - k')^2$: negative momentum transfer squared,

$W^2 = M_h^2 = (p + q)^2$: mass of the hadronic system in the final state,

$x = \frac{Q^2}{2p \cdot q}$: the fraction of the proton carried by the struck quark,

$y = \frac{p \cdot q}{p \cdot k}$: fraction of the electron momentum transferred to the proton in its rest system.

These variables are not all independent. They are connected by the relation $Q^2 = xys$. In inclusive DIS, there is a color flow between the struck quark and the proton remnant. As a consequence, hadrons will be produced in this angular region in particular at small angles w.r.t. the proton direction. In diffraction scattering, the situation is different as shown in Fig. 2.

Diffractive scattering is mediated by the exchange of a colorless object between the proton and the virtual photon. The proton remains intact and no color flow is connected with this exchange. As a consequence, a hadronic system X is created which is well separated from the proton. A large (pseudo)rapidity gap exists

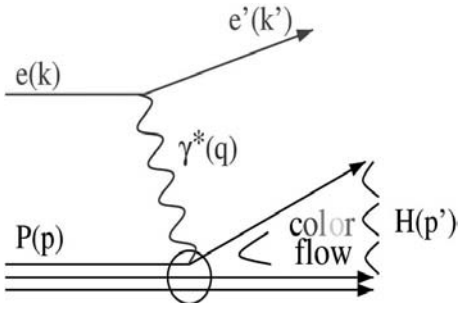

Fig.1. Diagram for inclusive deep inelastic e-p scattering

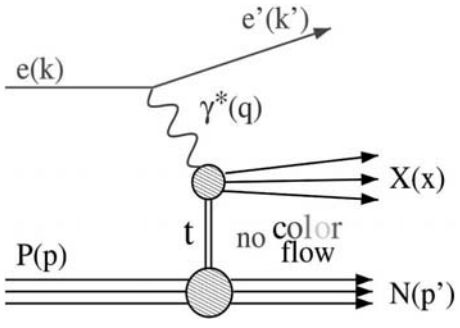

Fig.2. Diagram for diffractive e-p scattering

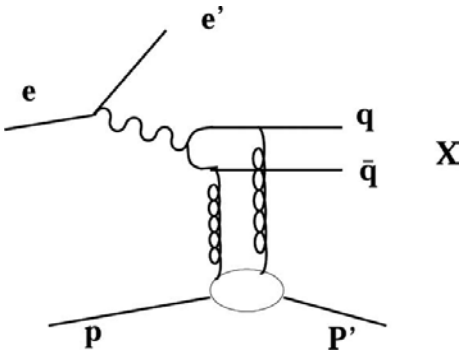

Fig.3. Diffractive e-p scattering in pQCD by 2 gluon exchange

between the proton and the system X. The pseudorapidity η is defined as:

$\eta = -\ln\tan(\Theta/2)$.

Here Θ is the angle between the proton direction, called forward, and the first detected particle from the system X. Additional variables are needed to describe diffractive scattering. The following ones are commonly used:

M_X: mass of the diffractively produced hadronic system X,

$t = (p - p')^2$: four momentum transfer squared at the proton vertex,

$x_{IP} = \frac{(p-p')\cdot q}{p\cdot q} = \frac{M_X^2+Q^2}{W^2+Q^2}$: fraction of the proton momentum carried by the exchanged object,

$\beta = \frac{Q^2}{2(p-p')\cdot q} = \frac{Q^2}{M_X^2+Q^2} = \frac{x}{x_{IP}}$: momentum fraction of the exchanged object that is involved in the scattering process.

2. Regge Phenomenology Versus Perturbative QCD

Diffractive hadronic reactions have been studied extensively in peripheral processes and can be described in the framework of Regge phenomenology. In Regge theory [2], the exchanged object between the proton and the diffractive system X is a 'Regge trajectory'. A Regge trajectory describes the exchange of a system of generalized particles with continuous spin but otherwise the same quantum numbers. Trajectories are parametrized to be linear

$\alpha_{\rm R}(t) = \alpha_{\rm R}(0) + \alpha' t$.

The trajectory which carries the quantum numbers of the vacuum is called the pomeron trajectory [3] and the exchanged object the pomeron. Diffractive cross-sections at high energies are of the form:

$$\frac{d\sigma}{dt} \propto e^{b(W)\cdot t} \left(\frac{W}{W_0}\right)^{4(\alpha_{IP}(t)-1)}$$

$$\sigma_{\rm tot} \propto \left(\frac{W}{W_0}\right)^{2(\alpha_{IP}(0)-1)}$$

with $b(W) = b_0 + 4\alpha' \ln\left(\frac{W}{W_0}\right) t$.

All the trajectories on which a known particle lie have an intercept $\alpha_{\rm R}(0)$ smaller than zero. The experimental fact that, at high energies, the cross-section for elastic scattering rises with energy required to invent a hypothetical new trajectory, the pomeron trajectory, with an intercept greater than zero. At high enough energies, this pomeron contribution will dominate because the contributions from all other Regge trajectories will die out with energy. From a fit to all peripheral hadronic scattering data, Donnachie and Landshoff [4] found the following universal parametrization of the pomeron trajectory:

$(t) = 1.08 + 0.25t.$

Processes which are described by this trajectory are called soft diffraction. The predictions from Regge theory for soft diffraction are a power law behavior of the total cross section as $\sigma(W) \propto W^{\delta}$ with $\delta \approx 0.22$ and an exponential drop of the differential cross section as a function of t whith an increasing slope, $b(W)$, as W increases. This last fact is called shrinkage. The slope parameter b is proportional to r^2 where r is a measure for the extension of the interacting objects. With increasing W, also r increases, which means that the scattering objects get bigger.

A description of diffractive deep inelastic scattering (hard diffraction) is given in Figs. 3 and 4. The virtual photon splits into a quark-antiquark pair and, in the simplest approach, two gluons which form a colorless object are emitted from the proton and couple to the quark-antiquark pair. In higher orders of pQCD, the exchanged gluon system is commonly treated as a BFKL-type ladder [5]. Various pQCD inspired models exist for hard diffractive scattering. All these models predict little or no shrinkage.

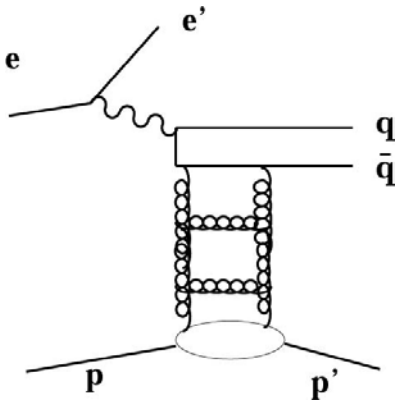

Fig.4. Diffractive e-p scattering in pQCD by BFKL-type ladder exchange

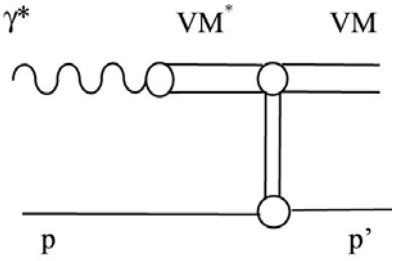

Fig.5. Exclusive vector-meson production in the VMD-Regge framework

3. Exclusive Vector-Meson Production

Exclusive vector-meson production is a diffractive process and has been studied extensively. The complete diffractively produced system, i.e. the final state vector-meson, can be detected. Theoretically, the vector-meson dominance model (VMD) [6] plus Regge theory provide a framework in which exclusive vector-meson production is understood as a quasi-elastic scattering where the incoming vector-meson is off mass-shell. The situation is graphically shown in Fig.5.

In pQCQ, exclusive vector-meson production proceeds according to Fig.6. The virtual photon splits into a quark-antiquark pair with relative momentum fractions z and $1-z$. In the lowest order, two gluons are exchanged between the proton and the quark-antiquark pair which recombines afterwards to form the vector-meson. The transverse separation, r, of the quark and antiquark is given in pQCD by:

$$r^2 = [z(1-z)Q^2 + m_q^2]^{-1} \ .$$

Here m_q is the mass of the quark(antiquark) of which the vector-meson is composed. Perturbative QCD is

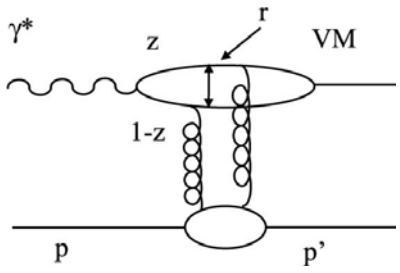

Fig.6. Exclusice vector-meson production as a pQCD process

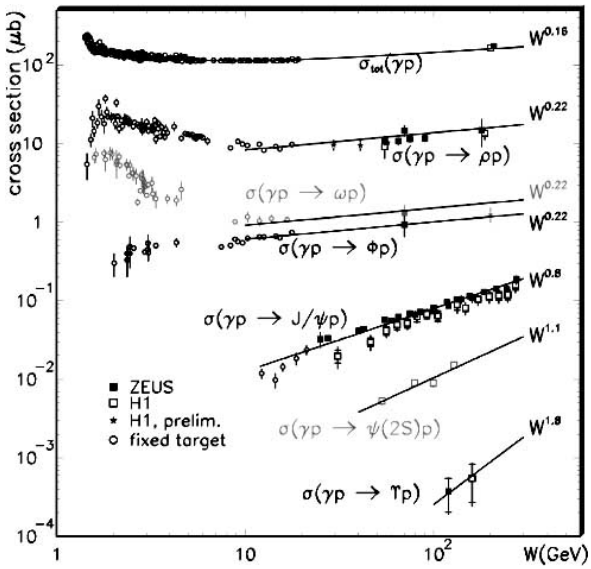

Fig.7. Photoproduction cross-section for ρ, ω, ϕ, J/Ψ, $\Psi(2S)$, and Υ

expected to be applicable when the transverse dimension, r, of the quark-antiquark system gets small. This happens when either Q^2 or m_q gets big. Perturbative QCD models predict a rise of the cross-section like $\sigma(W) \propto W^\delta$ with $\delta \approx 0.8$ which is faster than expected from Regge theory. The slope of the t-distribution is predicted to be $b \approx 4$ GeVand $\alpha' \approx 0$. This means no or little shrinkage. The conditions under which exclusive vector-meson production is a hard diffractive process that can be described by pQCD models will be investigated in the rest of this section.

3.1. Can the Vector-Meson Mass be a Hard Scale?

Data from photoproduction permit one to test the behavior of exclusive vector-meson production as a function of the meson mass because $Q^2 = 0$. Fig.7 shows the cross-sections for production of ρ, ω, ϕ, J/Ψ, $\Psi(2S)$,

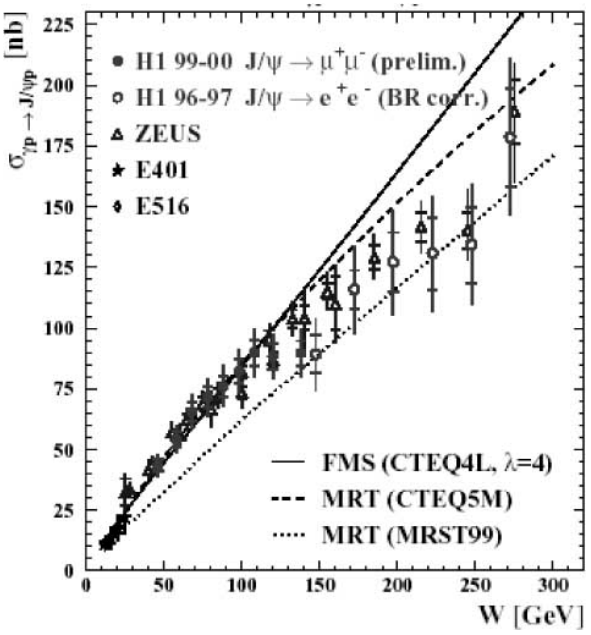

Fig.8. Cross-section of J/Ψ photoproduction as a function of W compared to pQCD models

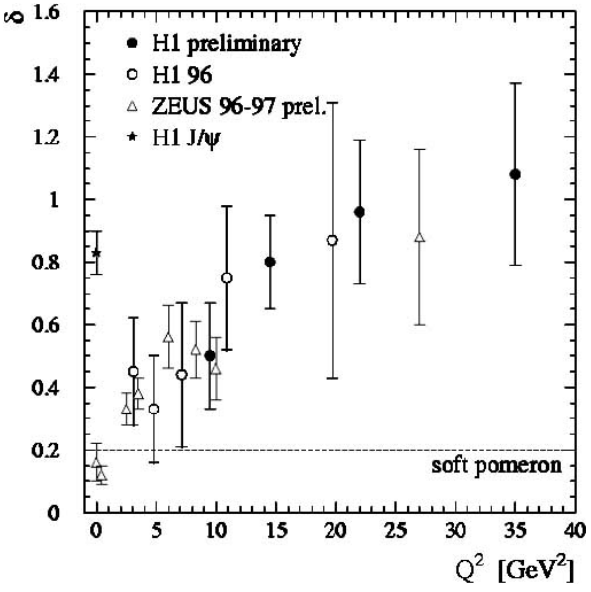

Fig.9. The slope δ of the W-dependence of DIS ρ production

and Υ as functions of W [7—12]. The lines through the data points are only to guide the eye and are no fit results.

The W-dependence of the light vector-mesons (ρ, ω, ϕ) can be described by a slope $\delta \approx 0.22$ in agreement

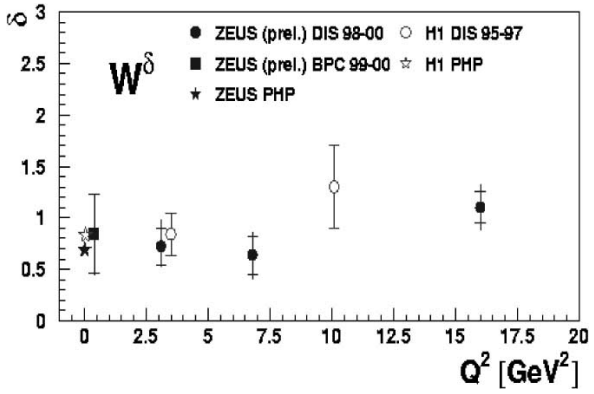

Fig.10. The slope δ of the W-dependence of DIS J/Ψ production

with Regge-phenomenology. For higher vector-meson masses, the rise with W gets steeper. This indicates the onset of hard diffraction. Therefore exclusive production of J/Ψ meson should be described by pQCD model calculations already from $Q^2 = 0$ on. In Fig.8, the photoproduction cross-section for J/Ψ mesons as a function of W is compared to pQCD model calculations [13]. These calculations are able to describe the data qualitatively.

3.2. Can Q^2 Provide a Hard Scale?

In the pQCD picture of vector-meson production, the interacting objects get smaller with increasing Q^2. One therefore expects that this becomes a hard process at high Q^2 and the application of pQCD models is justified. Fig.9 shows the slope of the W-dependence as a function of Q^2 for DIS ρ production [14]. Starting from a value compatible with a soft Pomeron trajectory, it rises with Q^2 to considerably higher values. For DIS J/Ψ production [15], the W-slope is independent of Q^2 at a value not compatible with a soft pomeron trajectory. This is shown in Fig.10. The δ-value for J/Ψ production is approximately equal to the value for ρ production at high Q^2.

Another parameter which is supposed to change in the transition from the Regge regime to pQCD is the slope b of the t-distribution. The Figs. 11 and 12 show this slope as a function of Q^2 for ρ- and J/Ψ-production. For ρ-production, the t-slope decreases with increasing Q^2 to a value of about 4 as expected from pQCD models. For J/Ψ-production, this slope is constant with Q^2 at the level of about 4 which reflects the fact that J/Ψ-production is a hard process from $Q^2 = 0$ on. One concludes that the initially soft ρ-production becomes a hard process with increasing Q^2.

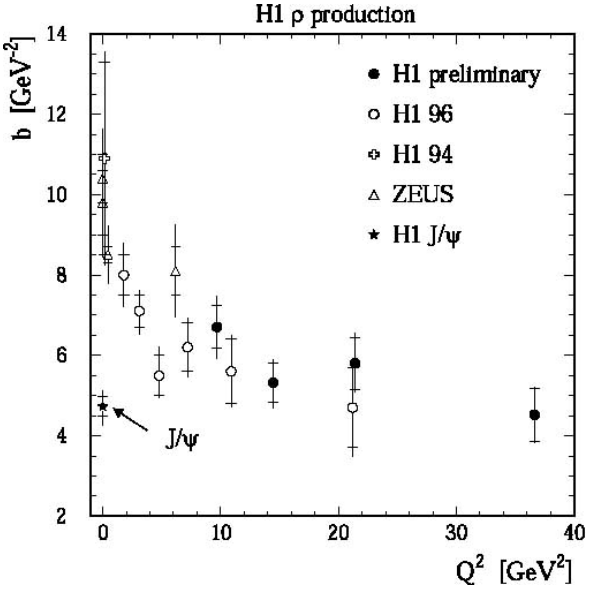

Fig.11. The t-slope parameter b of DIS ρ production as a function of Q^2

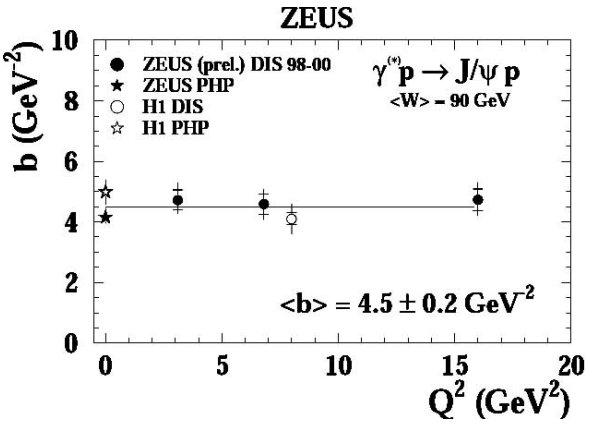

Fig.12. The t-slope parameter b of DIS J/Ψ production as a function of Q^2

Finally, Fig.13 shows the cross section for J/Ψ-production as a function of Q^2. The data are well described by pQCD models [16, 17] even from $Q^2 = 0$ on. These models use parton-density functions derived from inclusive deep inelastic scattering. An empirical fit of the form $(Q^2 + M_{J/\Psi})^{-n}$ with $n = 2.72 \pm 0.10$ also describes the data at higher values of Q^2.

3.3. Can | t | Provide a Hard Scale?

In a similar way as the square of the momentum transfer from the electron to the vector-meson, Q^2, leads

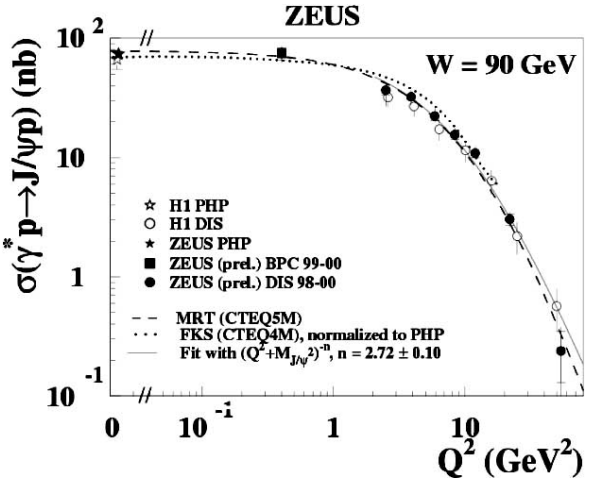

Fig.13. The cross section of J/Ψ production as a function of Q^2. The data are compared to pQCD models

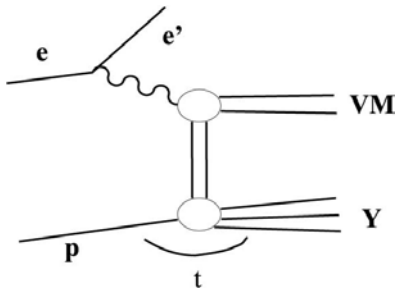

Fig.14. Schematic diagram of vector-meson production with proton dissociation

eventually to a hard scale which justifies the application of pQCD one would expect that also the square of the momentum transfer from the proton to the vector-meson, $\mid t \mid$, can serve as a hard scale. To study this, photoproduction of vector-mesons at high $\mid t \mid$ has been investigated. Experimentally, this leads to a small complication. All studies presented so far have been performed with data integrated over $\mid t \mid$. Since the $\mid t \mid$-dependence is exponentially falling, mainly very small $\mid t \mid$-values dominated the data. At higher $\mid t \mid$-values, it becomes more and more likely that the proton will not stay intact but will dissociate into a hadronic system as shown in Fig 14.

At a low mass of the hadronic system Y, e.g. Y being a nuclear resonace, the particles emerging from this system will leave the detector under very small angles through the beam pipe without being registered. These events cannot be distinguished experimentally

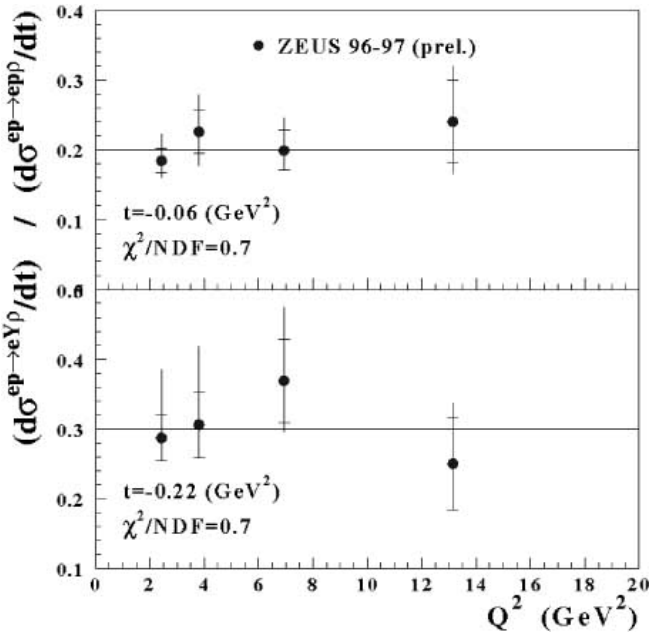

Fig.15. The ratio of proton dissociative to proton nondissociative cross sections

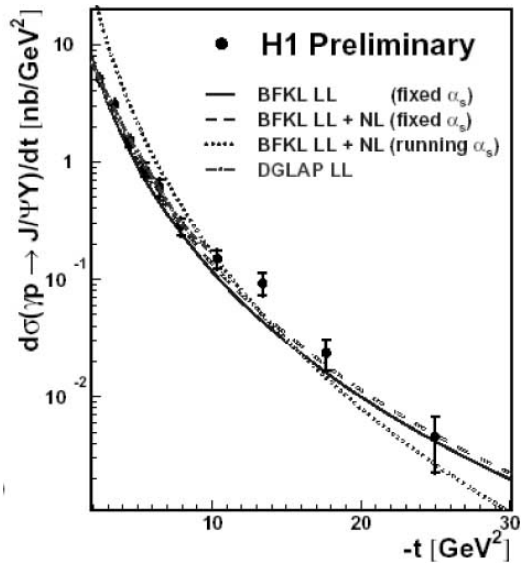

Fig.17. Differential cross-section as a function of t for proton dissociative photoproduction of J/Ψ mesons from the H1 experiment

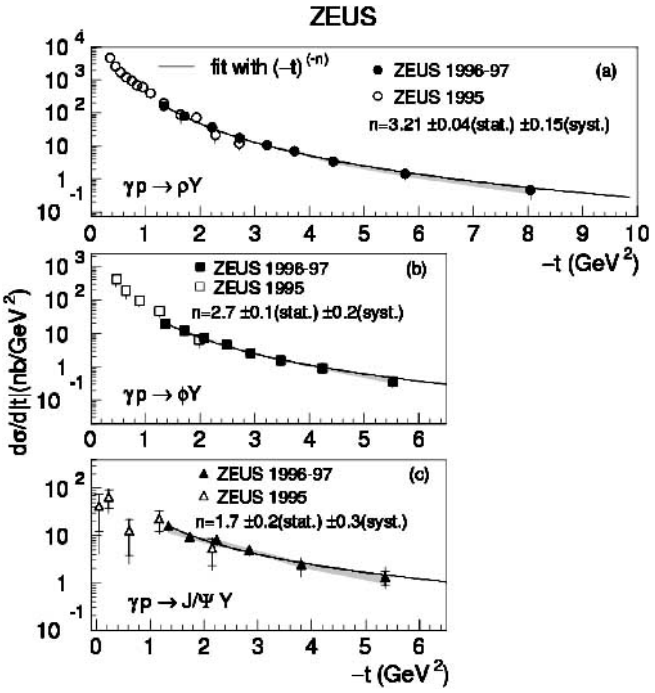

Fig.16. Differential cross-section as a function of t for proton dissociative photoproduction of vector-mesons from the ZEUS experiment

from events in which the proton stayed intact. At higher masses of Y, some of the particles emerge with high enough transverse momenta to be seen in the detector. These events can be recognized and excluded from the dataset. Thus, at higher $\mid t \mid$values, one deals with the mixture of proton dissociatives and nondissociative processes. At high $\mid t \mid$ values, the proton dissociative events finally dominate. In order to draw conclusions from such events for the process of diffraction, one has to assume vertex factorization, i.e. that the ratio $\sigma_{\gamma p \to \rho Y}/\sigma_{\gamma p \to \rho p}$ only depends on M_Y, W, and t and not on Q^2. Data on this ratio are shown in Fig.15. Within the experimnetal errors, vertex factorization holds.

In Fig.16, t-distributions are shown for proton dissociative photoproduction of ρ, ϕ, and J/Ψ mesons from ZEUS. The data are well described by fits of the form:

$$\frac{d\sigma_{\gamma p \to VY}}{dt} \propto \mid t \mid^{-n} \quad .$$

The fit results for the exponents are given in the figures. The data are also compared to the pQCD models of Bartels et al. [18] and Ivanov et al. [19]. Data from H1 on proton dissociative photoproduction of J/Ψ meson are displayed in Fig.17. Here, the data are compared to pQCD fits according to BFKL and DGLAP. It follows from the H1 and ZEUS data that photoproduction of vector-mesons at high $\mid t \mid$ is well described by pQCD calculations. Also large $\mid t \mid$ provides a hard scale.

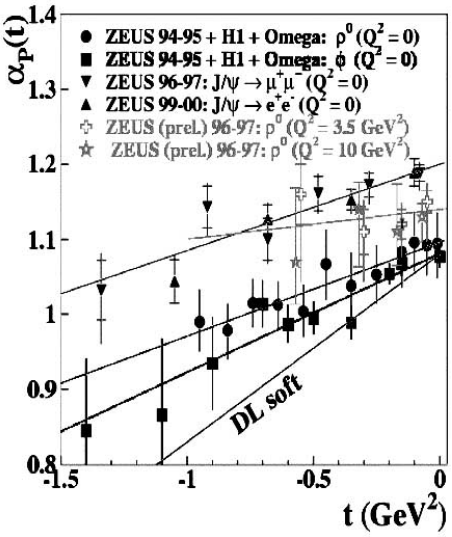

Fig.18. Pomeron trajectories

3.4. Pomeron Trajectory

Staying within the framework of Regge theory, the best way to determine the pomeron trajectory is to extract $\alpha_{I\!P(t)}$ for different t-bins from the W dependence of the data according to:

$$\frac{d\sigma}{dt} \propto e^{b(W)t} \left(\frac{W}{W_0}\right)^{4(\alpha_{I\!P}(t)-1)} .$$

Fig.18 shows the so-determined pomeron trajectories for photoproduction of ρ, ϕ, and J/Ψ as well as the one from DIS ρ production and the soft pomeron trajectory. The following trajectories are derived from the data:

$$\begin{aligned}
&\rho \text{ photoproduction} &: \alpha_{I\!P}(t) &= 1.10 + 0.13t ,\\
&\phi \text{ photoproduction} &: \alpha_{I\!P}(t) &= 1.08 + 0.16t ,\\
&\text{DIS } \rho \text{ production} &: \alpha_{I\!P}(t) &= 1.14 + 0.04t ,\\
&J/\Psi \text{ photoproduction} &: \alpha_{I\!P}(t) &= 1.20 + 0.12t ,\\
&\text{soft pomeron} &: \alpha_{I\!P}(t) &= 1.08 + 0.25t .
\end{aligned}$$

The $\alpha_{I\!P}(0)$ values of ρ and ϕ photoproduction are compatible with the soft pomeron trajectory. The $\alpha_{I\!P}(0)$ values of DIS ρ and J/Ψ production are definitely higher.

3.5. Dipole-Pomeron Model

So far all the experimental evidence suggests that when a hard scale is involved in the production of vector-mesons, pQCD models can describe the data whereas the soft pomeron description fails. It is still possible to describe the data by the exchange of a pomeron-like trajectory but the parameters of that trajectory depend on the hard scale and on the process. More sophisticated models in which the exchange of a pomeron trajectory is generalized may also explain the data. An example is the Dipole-Pomeron model by Martynov, Predazzi and Prokudin [21]. In this model, the amplitude of the pomeron exchange contains two contributions:

$$A_{I\!P} = ig_0 \left(\frac{-is}{s_0}\right)^{\alpha_{I\!P}(t)-1} +$$

$$+ig_1 \ln\left(\frac{-is}{s_1}\right)\left(\frac{-is}{s_1}\right)^{\alpha_{I\!P}(t)-1}$$

with

$$\alpha_{I\!P}(t) = 1.0 + 0.25t .$$

This model is able to describe the data on exclusive photoproduction and DIS production of vector-mesons as shown in Fig.19 and Fig.20.

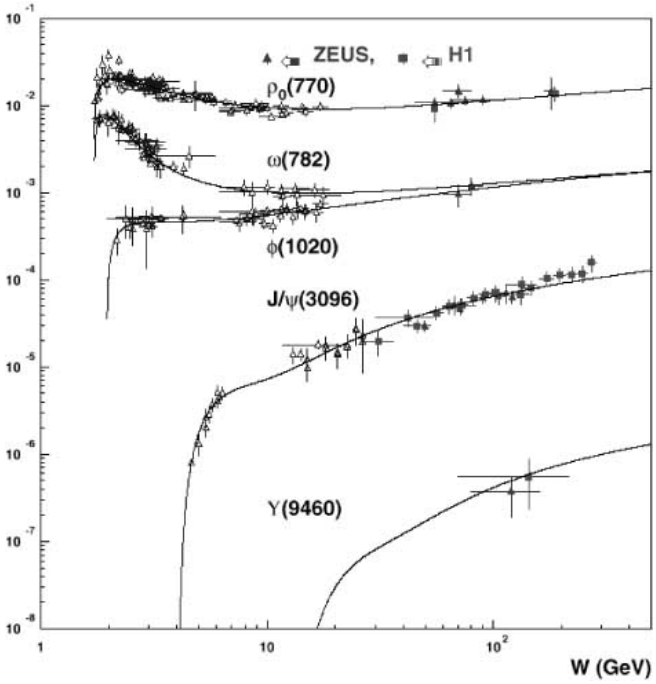

Fig.19. Cross-sections for the exclusive photoproduction of vector-mesons compared to the Dipole-Pomeron model of Martynov, Predazzi and Prokudin

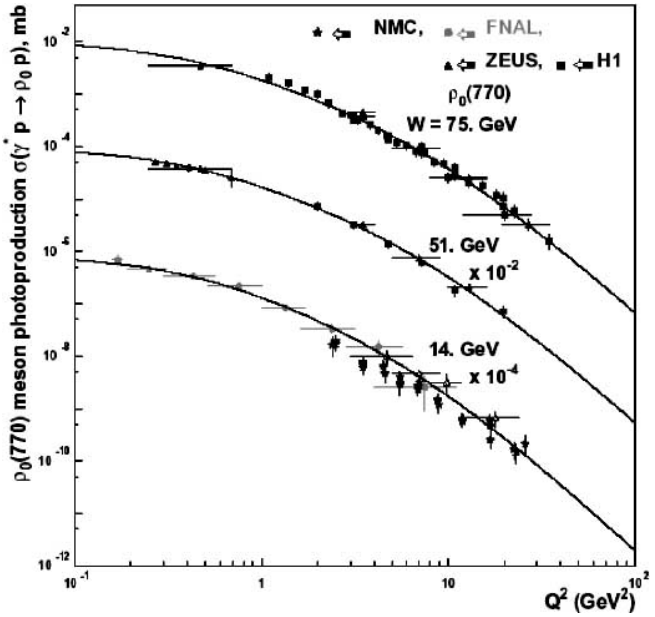

Fig.20. Cross-sections for the DIS exclusive ρ production compared to the Dipole-Pomeron model of Martynov, Predazzi and Prokudin

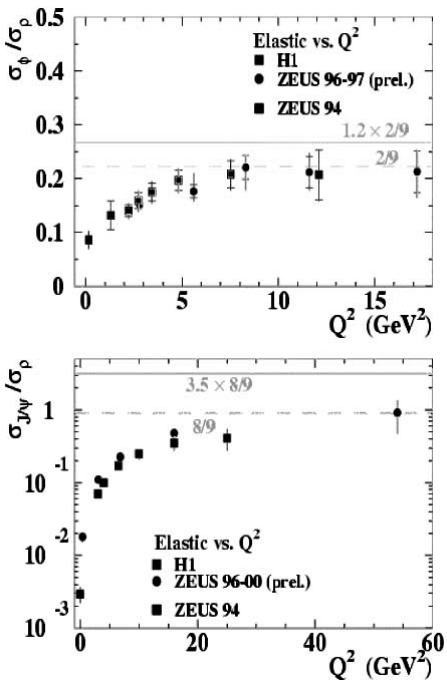

Fig.21. Upper part : ratio of cross-sections for the production of ϕ mesons to ρ mesons as a function of Q^2. Lower part : ratio of cross-sections for the production of ϕ mesons to ρ mesons as a function of Q^2

3.6. Ratios of Vector-Meson Production Cross-Sections

In the VMD+Regge framework, the ratios of exclusive vector-meson production cross-sections are determined by the couplings of the photon to the vector-mesons. The latter is given by the electrical charges of the quarks in the vector-meson according to SU(4). From this, one expects the following ratios of cross-sections:

$$\rho : \omega : \Phi : J/\Psi = 9 : 1 : 2 : 8 .$$

In pQCD, the cross section for longitudinal photons is given by [22]:

$$\frac{d\sigma^L_{\gamma^* p \to VMp}}{dt} =$$

$$= \Gamma_{VM \to e^+e^-} M_{VM} \eta^2_{VM} \frac{\alpha_{ss}(Q^2_{\rm eff}) \left[xg(x, Q^2_{\rm eff})\right]^2}{Q^6}.$$

Here, η_{VM} is the integrated wave function of the vector-meson which can be assumed to be universal at high Q^2. In pQCD, one therefore expects

$$\frac{\sigma_{VM1}}{\sigma_{VM2}} = \frac{\Gamma_{VM1}}{\Gamma_{VM2}} \frac{M_{VM1}}{M_{VM2}}$$

and consequently

$$\rho : \omega : \Phi : J/\Psi = 9 : 1 \cdot 0.8 : 2 \cdot 1.2 : 8 \cdot 3.5 =$$

$$= 9 : 0.8 : 2.4 : 28.1 .$$

The simple SU(4) relation is not expected to hold in pQCD. Fig. 21 shows the measured cross-section ratios σ_ϕ/σ_ρ and $\sigma_{J/\Psi}/\sigma_\rho$ as functions of Q^2.

For $Q^2 > 8$ GeV^2, the ratio of ϕ production to ρ production reaches the simple SU(4) prediction. It might still be compatible with the pQCD expectation at higher Q^2.

Even at high Q^2, the ratio of J/Ψ production to ρ production is compatible with the SU(4) prediction rather than with the pQCD expectation. Note the logarithmic scale of the plot. Present pQCD-models do not reproduce the ratio of J/Ψ production to ρ production.

3.7. Ratios of Vector-Meson Production to the Total Cross Section

In the Regge framework as well as in pQCD, the amplitude for exclusive vector-meson production is predicted to rise proportionally to W^δ and the cross-section therefore is proportional to $W^{2\delta}$. The total

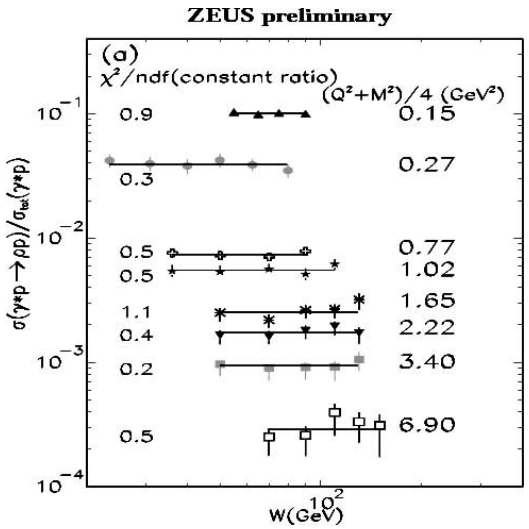

Fig.22. Ratio of the ρ production cross section to the total virtual photon-proton cross-section as a function of W for different values of $(Q^2 + M_\rho^2)/4$

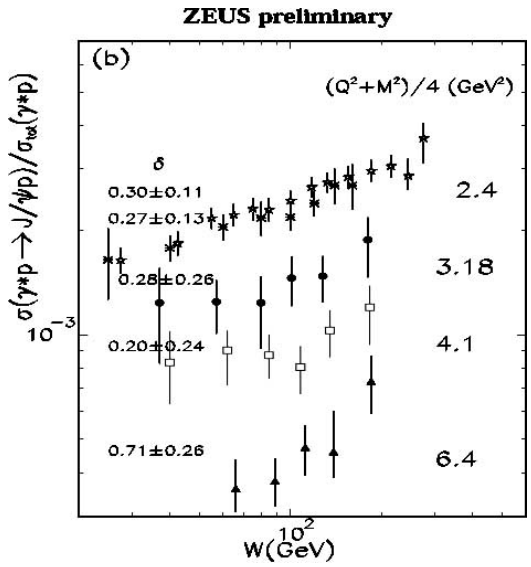

Fig.23. Ratio of the J/Ψ production cross-section to the total virtual photon-proton cross-section as a function of W for different values of $(Q^2 + M_{J/\Psi}^2)/4$.

virtual photon-proton cross-section is, according to the optical theorem, proportional to the imaginary part of the elastic forward scattering amplitude. In the VMD-model, the photon is represented as a sum over the vector-mesons. Therefore, the total virtual photon-proton cross-section is expected to be proportional to W^δ. This leads to:

$$\frac{\sigma(\gamma^\star p \to V M p)}{\sigma_{\rm tot}(\gamma^\star p)} \propto \frac{W^{2\delta}}{W^\delta} \propto W^\delta \ .$$

The measured ratios for ρ production and J/Ψ production, are shown in Figs. 22 and 23.

For the J/Ψ-production, the ratio rises as expected with W. However, for ρ-production, the ratio is about constant for all values Q^2. This is in contrast to the expectations from VMD and optical theorem.

3.8. Helicity Structure of Exclusive Vector-Meson Production

For the exclusive vector-meson production, the complete final state is measured except the scattered proton. Therefore one can determine the angular correlations of initial and final state particles. This enables an analysis of the spin structure of the reaction. Fig. 24 defines the relevant angles for exclusive ρ production. For ρ production, three angles determine the spin structure of the process: the angle Φ between the lepton scattering plane and the ρ production plane, the angle ϕ between the ρ production plane and the ρ decay plane, and the

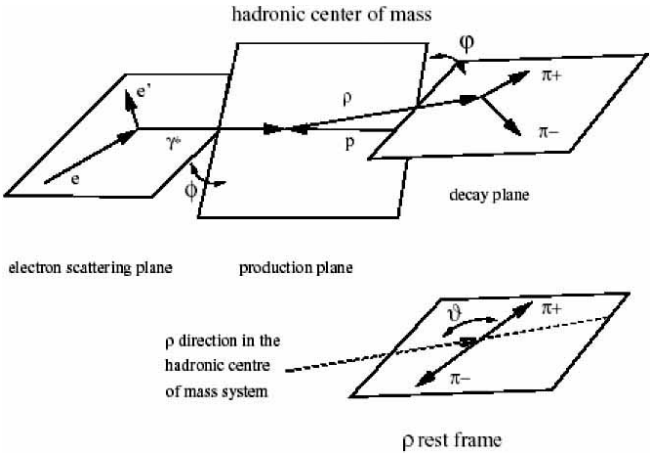

Fig.24. Definition of angles which determine the spin structure of the process for exclusive ρ production

angle θ in the ρ rest frame between the ρ momentum direction and the direction of the π^+ decay particle. The complete angular correlations are given by a function of 15 parameters [23]: $W(\Phi, \phi.\theta) = f(r_{ij}^{kl})$.

The 15 parameters r_{ij}^{kl} are related to helicity amplitudes $T_{\lambda_{VM}\lambda_\gamma}$. For example: r_{00}^{04} gives the probability for a single spin flip, r_{1-1}^{04} is the interference between the helicity non flip and double flip, and $\mathrm{Re}(r_{10}^{04})$ is the interference between helicity non flip and single flip.

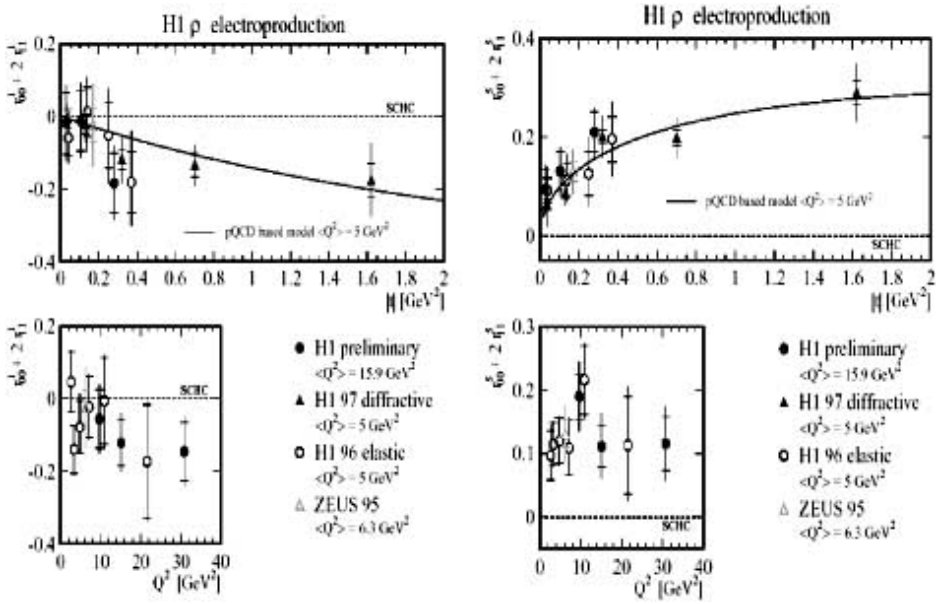

Fig.25. Ratio of the ρ production cross-section to the total virtual photon-proton cross-section as a function of W for different values of $(Q^2 + M_\rho^2)/4$

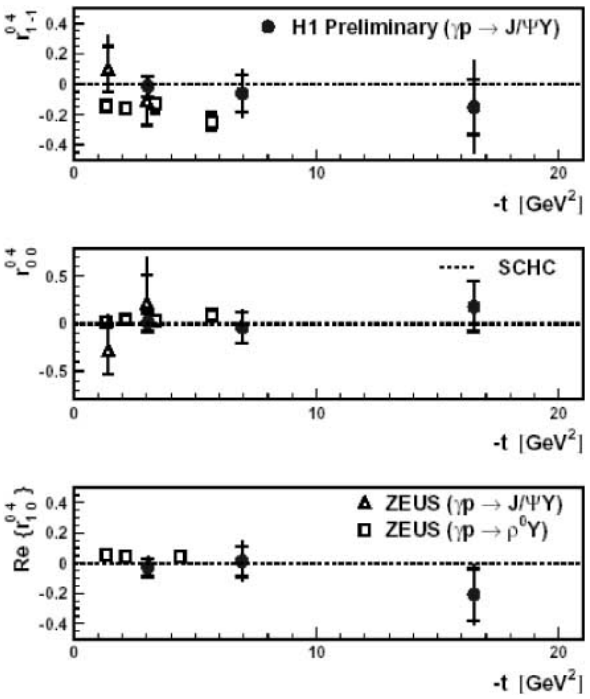

Fig.26. Ratio of the J/Ψ production cross-section to the total virtual photon-proton cross-section as a function of W for different values of $(Q^2 + M_{J/\Psi}^2)/4$

For J/Ψ production, the parameters are not the same and have different meanings because the J/Ψ decays into spin $1/2$ particles.

A widespread assumption in vector-meson production is the S-channel helicity conservation (SCHC) which means that the helicity of the virtual photon is taken over by the produced vector-meson. Under this assumption, combinations of parameters which give a nonzero probability for single or double spin flip should vanish. Figs. 25 and 26 show such combinations for ρ and J/Ψ production as functions of t.

For ρ production, the combination $r_{00}^1 + 2r_{11}^1$ gives the probability for double spin flip processes and $r_{00}^5 + 2r_{11}^5$ for single spin flip ones. It is obvious that SCHC is violated at high $\mid t \mid$ because these two combinations of parameters differ from zero significantly. For J/Ψ production, however, the data for the combinations which are expected to vanish for SCHC are compatible with zero even at high $\mid t \mid$.

From the measured spin density matrix elements, one can extract the transverse and longitudinal cross-sections of vector-meson production. In Fig.27, the cross-sections for ρ production by transverse photons, σ_T, and by longitudinal photons, σ_L, are shown as functions of Q^2. At high Q^2, the longitudinal cross-section is considerably higher than the transverse one. In Fig.28, the ratio of transverse to longitudinal cross-section is shown. This ratio can be expressed in terms of spin density matrix elements:

$$R = \frac{\sigma_L}{\sigma_T} \approx \frac{r_{00}^{04}}{\epsilon(1 - r_{00}^{04})}$$

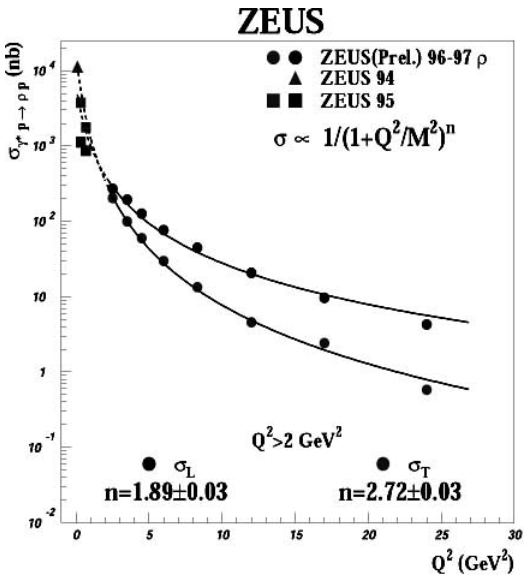

Fig.27. The transverse cross-section (lower curve) and the longitudinal cross-section (upper curve) for exclusive ρ production versus Q^2

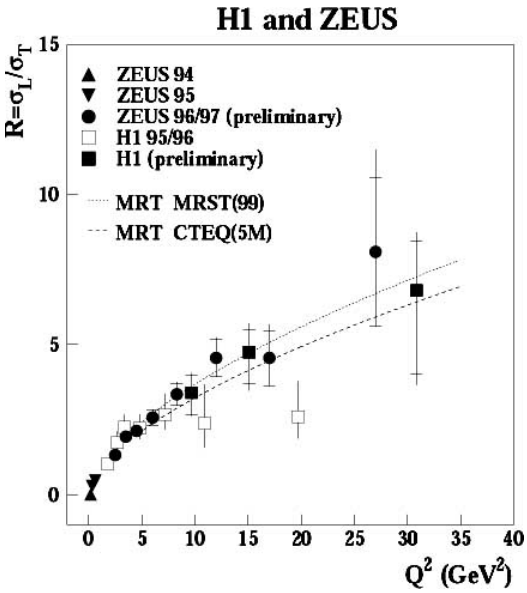

Fig.28. Ratio of the longitudinal to transverse cross-section for exclusive ρ production versus Q^2 compared to pQCD-models [24]

with

$$\epsilon = \frac{2(1-y)}{1+(1-y)^2} \ .$$

The fact that $R = \sigma_L/\sigma_T$ is much bigger than 1 at higher Q^2 is a justification for the fact that previously only the longitudinal cross sections in pQCD models have been considered.

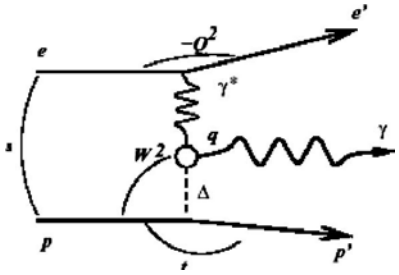

Fig.29. The graphical description of deeply virtual Compton scattering (DVCS)

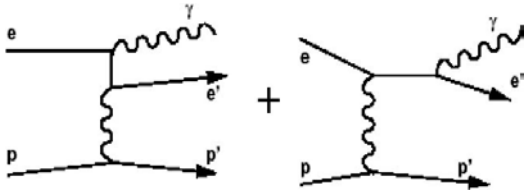

Fig.30. The graphs of Bethe-Heitler reactions which have the same final state as DVCS

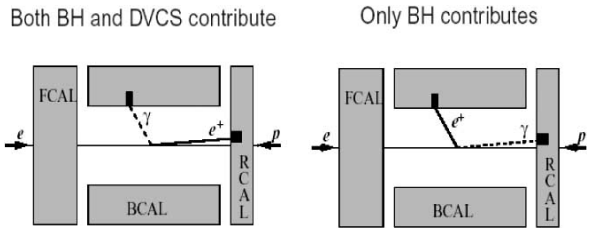

Fig.31. Experimental topologies to which Bethe-Heitler and DVCS processes contribute

4. Deeply Vitual Compton Scattering

Deeply virtual Compton scattering [25] is the QCD process described in Fig.29. A virtual photon scatters off the proton and appears as a real photon in the final state. This is a process very close to true elastic scattering. There exist, however, Bethe — Heitler reactions, radiation of photons from the incoming and outgoing leptons, which lead to the same final state. This is shown in Fig. 30.

The measurement of the DVCS cross-section is an experimental challenge because the Bethe — Heitler cross-section is much larger than the DVCS one. In Fig.31, the two possible final state topologies are shown. In the case where the lepton appears under a small scattering angle, both Bethe — Heitler and DVCS processes contribute. The topology in which the photon appears under the smaller scattering angle is only

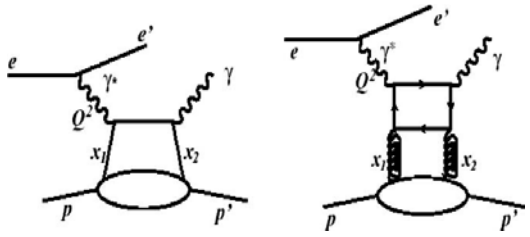

Fig.32. QCD diagrams which contribute to deeply virtual Compton scattering

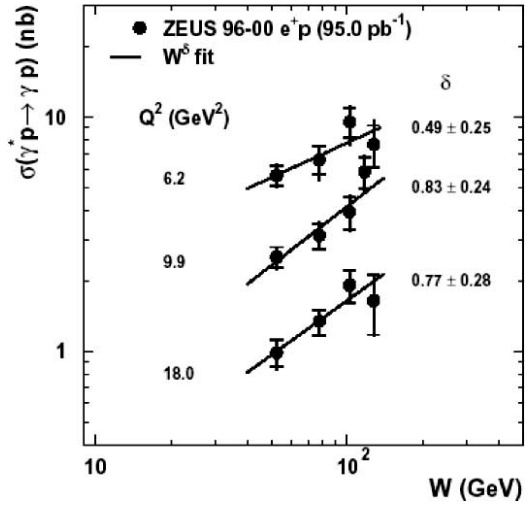

Fig.33. The DVCS cross-section as a function of W for various values of Q^2

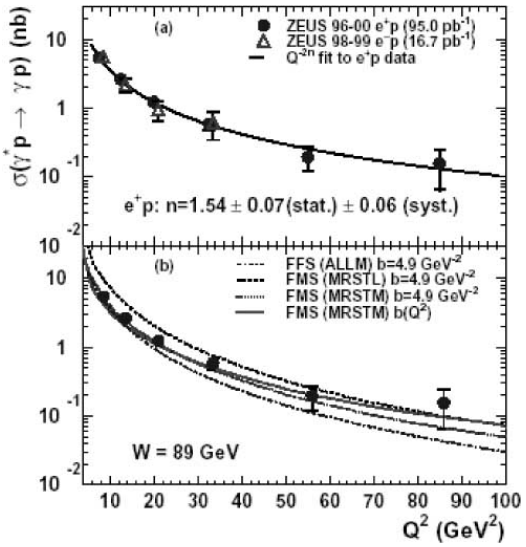

Fig.34. The DVCS cross-section as a function of Q^2. The data are compared to pQCD models

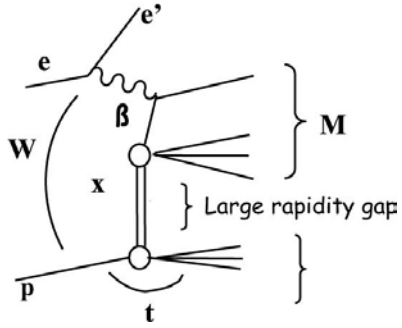

Fig.35. Diagram for inclusive diffractive scattering when the pomeron has a partonic structure

populated by the Bethe — Heitler process. In this way the Bethe — Heitler rate can be measured, extrapolated, and subtracted to receive the pure DVCS rate. The interference of the QED and QCD processes gives access to the real part of the QCD amplitude, $\mathrm{Re}A_{\mathrm{QCD}}$. In lowest order of pQCD, two diagrams contribute to the DVCS process. They are shown in Fig.32.

A novel feature appears here. The two partons, emitted and reabsorbed by the proton, are at different values of Bjorken x. This leads to generalized parton distributions (GPD) [26]. The data for DVCS [27] are shown in Figs. 33 and 34. They are compared to pQCD models based on generalized parton distributions. These models can describe the W- and Q^2-dependence well. The W-dependence is stronger than the expected one from a soft pomeron exchange. The available experimental data are not yet sufficient to measure angular distributions from which the interference term could be extracted.

5. Inclusive Diffraction

The process of inclusive diffraction is illustrated in Fig.35 in the picture in which the Pomeron has a partonic structure [28]. The virual photon scatters off one quark/antiquark in the pomeron. The scattered quark/antiquark together with the remainder of the pomeron form the diffractively produced system X. The proton may dissociate in a low mass hadronic system Y of which most particles will escape detection in the very forward direction.

The two variables $x_{I\!P}$ and β acquire the following meaning in the partonic Pomeron picture:

$$x_{I\!P} = \frac{M_X^2 + Q^2}{W^2 + Q^2}$$

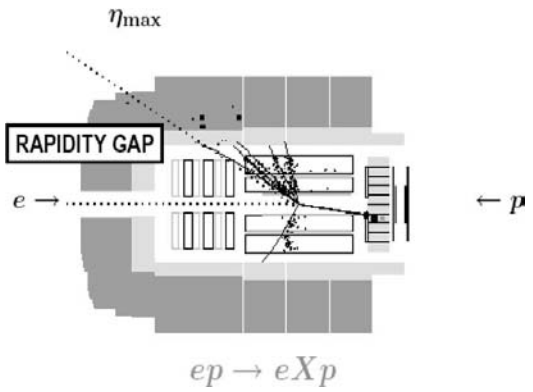

Fig.36. A large rapidity gap event in the H1 detector

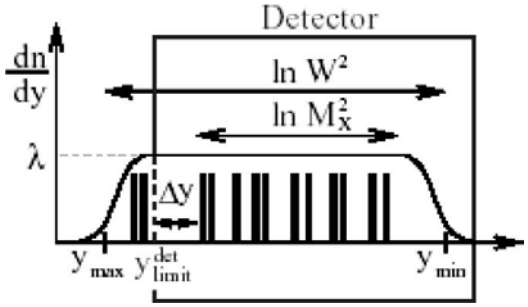

Fig.37. Rapidity distribution for nondiffractive events. Indicated is the full length of the rapidity plateau, the acceptance limits of a detector and a possible rapidity gap due to statistical fluctuations

momentum fraction of the proton carried by the pomeron

$$\beta = \frac{x}{x_{IP}} = \frac{Q^2}{M_X^2 + Q^2}$$

momentum fraction of the pomeron carried by the struck quark.

There are essentially two ways to select inclusive diffraction events experimentally.

1.) The η_{max}- method :

This method makes explicit use of the rapidity gap in a diffractive event as shown in Fig.36. A measure of the rapidity gap is the maximum pseudorapidity seen in the detector from a track or an energy deposit in the calorimeter.

$$\eta_{max} = -\ln \tan(\Theta_{min}/2).$$

Here Θ_{min} is the angle of the most forward detected track or energy deposit. Requesting an η_{max}-value smaller than a certain value selects diffractive events with a minimum rapidity gap. The η_{max}- method is used by the H1 collaboration.

2.) The M_X-method [30]:

This method exploits the different shapes of the $\ln M_X^2$ distributions for nondiffractive and diffractive events.

(i) Nondiffractive events:

The rapidity of a produced particle is defined as $y = \frac{1}{2}\ln\frac{E+p_z}{E-p_z}$ where E is the particle's energy and p_z its longitudinal momentum. For a given center of mass energy W of the reaction, maximum and minimum values of the rapidity are related to W by $W^2 = c_0 \exp(y_{max} - y_{min})$. The real detector has a limited acceptance and particles from the proton remnant in the very forward direction leave the detector unmeasured. The acceptance starts only at y_{limit}. The mass of the detected hadronic system is then given by $M_X^2 = c_0 \exp(y_{limit} - y_{min})$. This is sketched in Fig.37.

For uncorrelated particle emission in nondiffractive events, the rapidity distribution is flat [29]:

$$\frac{dN_{part}}{dy} = \lambda = \text{const.}$$

The Poisson probability to find no particle in a region Δy close to the proton direction is given by:

$$P(0) = e^{-\lambda \Delta y} .$$

This leads to a $\ln M_X^2$-distribution of the form:

$$\frac{dN_{nondiff}}{d\,\ln M_X^2} = c e^{b \ln M_X^2} .$$

The slope b must be determined from data. An experimental $\ln M_X^2$-distribution is shown in Fig.38. The slope b is indicated as a line rising with $\ln M_X^2$. Ideally this rise continues to the highest $\ln M_X^2$-value but, in reality, the detector effects make the distribution turn over and go to zero.

(ii) Diffractive events:

It has been found experimentally that, at high energies for diffractive events with not too low M_X, the following relation is valid:

$$\frac{dN_{diff}}{d\ln\, M_X^2} \propto \frac{1}{(M_X^2)^n} \qquad \text{with} \qquad n \approx 1 .$$

This leads to a flat $\ln M_X^2$-distribution:

$$\frac{dN_{diff}}{d\ln M_X^2} = D + c e^{b \ln\, M_X^2}$$

for

$$\ln M_X^2 \leq \ln W^2 - \eta_0 .$$

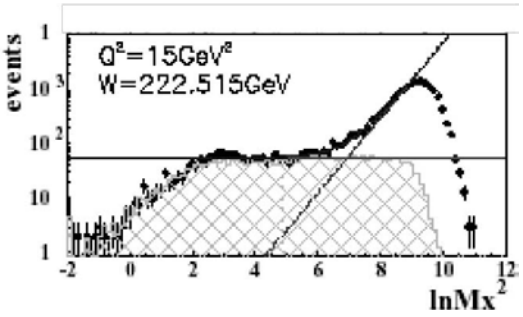

Fig.38. Measured $ln\ M_X^2$-distribution. The cross hatched area shows the MC simulated contribution from diffractive events. The horizontal line is the height of the diffractive plateau. The other line shows the exponential fall off of the nondiffractive contribution

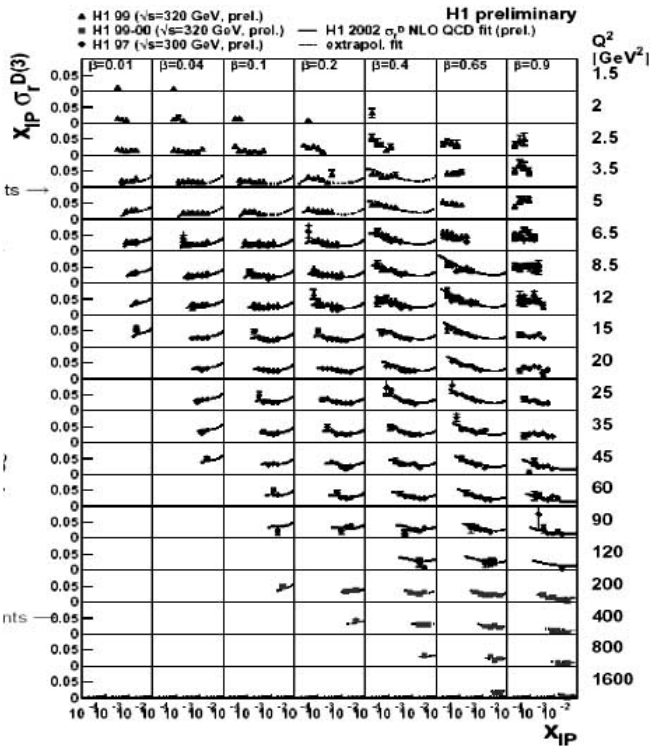

Fig.39. H1 results on the reduced diffractive cross-section multiplied by x_{IP} as a function of x_{IP} for values of Q^2 from 1.5 GeV^2 to 1600 GeV^2 and β from 0.01 to 0.90

An MC-simulation of the diffractive contribution is also shown in Fig.38 where the constant D is represented by the horizontal line. For the extraction of the number of diffractive events, the slope b of the distribution of nondiffractive events has been fitted to the data, the number of nondiffractive events has been evaluated and then subtracted from the total number of events.

5.1. Diffractive Cross-Section and Diffractive Structure Functions

The differential cross section for diffractive processes can be expressed in terms of a diffractive structure function:

$$\frac{d^4\sigma}{dQ^2 dt dx_{IP} d\beta} =$$

$$= \frac{2\pi\alpha_{em}}{\beta Q^2}[1-(1-y)^2]F_2^{D(4)}(Q^2,t,x_{IP},\beta)\ .$$

Here the contribution from the longitudinal structure functions has been neglected. Also used by the H1 Collaboration is the reduced diffractive cross-section:

$$\sigma_r^D = F_2^D - \frac{y^2}{1+(1-y)^2}F_L^D\ .$$

In diffractive deep inelastic scattering, QCD factorization of the following form has been proven [31]:

$$\sigma^{\rm diff} \propto f_q^{\rm diff}(Q^2,t,x_{IP},\beta)\hat{\sigma}_{pQCD}\ .$$

Here $f_q^{\rm diff}(Q^2,t,x_{IP},\beta)$ are universal diffractive parton densities and $\hat{\sigma}_{pQCD}$ is the perturbatively calculable cross-section for the hard parton-parton scattering. Another factorization is commonly used in the picture where the pomeron has a partonic sructure [28]:

$$\sigma_{\rm diff} \propto f_{IP/p}(t,x_{IP})\cdot F_2^{IP}(Q^2,\beta).$$

The diffractive cross-section can be expressed by a pomeron structure function F_2^{IP} and a pomeron flux factor which comes from Regge theory:

$$f_{IP/p}(t,x_{IP}) = \frac{e^{Bt}}{x_{IP}^{2\alpha(t)-1}}\ .$$

This Regge factorization is an assumption. No proof exists for it.

5.2. Results on Inclusive Diffraction

Figs. 39 and 40 show the results of the H1 collaboration [32] and the ZEUS collaboration [33] on inclusive diffractive reactions. In Fig.39, the reduced diffractive cross section multiplied by x_{IP} is presented as a function of x_{IP} for values of Q^2 from 1.5 GeV^2 to 1600 GeV^2 and β from 0.01 to 0.90. The data are from different running periods. They are compared to a H1 LNO QCD fit which describes the data in general well. In Fig.40, the ZEUS measurements of $\frac{d\sigma^{\rm diff}}{dM_X}$ are given as a function of W for Q^2-values from 2.7 to 55 GeV^2 and for M_X-values from 1.2 to 30 GeV. All the results and conclusions presented

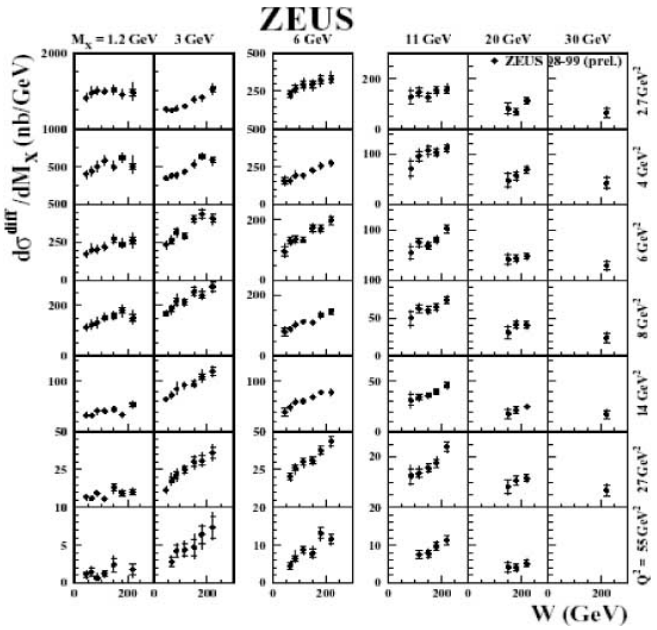

Fig.40. ZEUS measurements of $\frac{d\sigma^{\rm diff}}{dM_X}$ as functions of W for Q^2-values from 2.7 GeV^2 to 55 GeV^2 and for M_X-values from 1.2 GeV to 30 GeV

in the next sections are derived from these basic measurements.

5.3. Is Inclusive Diffraction a Soft Process?

The H1 Collaboration have fitted their results on the reduced cross-section by contributions from pomeron- and reggeon-exchanges according to:

$$\sigma_r^{D(3)}(Q^2, x_{I\!P}, \beta) =$$

$$= f_{I\!P}(x_{I\!P}) A(Q^2, \beta) + f_{I\!R}(x_{I\!R}) A_{I\!R}(Q^2, \beta)$$

with

$$f_{I\!P,I\!R} = \int_{-1}^{t_{\min}} \frac{e^{B_{I\!P,I\!R}\, t}}{x_{I\!P}^{2\alpha_{I\!P,I\!R}(t)-1}} \; .$$

The extracted intercept of the pomeron trajectory is shown in Fig.41 for three values of Q^2 together with the line representing the values derived from inclusive DIS and the soft pomeron line. The F_L^D contribution has been assumed to be zero. The band over the results shows the possible variation for $0 < F_L^D < F_2^D$. For Q^2-values above 10 GeV^2, the intercept of the pomeron trajectory clearly deviates from the soft pomeron expectation. The ZEUS data have been fitted to the functional form

$$\frac{d\sigma^{\rm diff}_{\gamma^* p \to XN}}{dM_X} = h W^{a^{\rm diff}} \propto (W^2)^{(2\overline{\alpha_{I\!P}}-2)} \; .$$

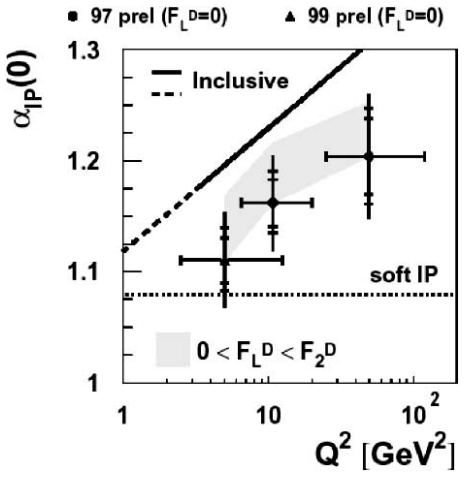

Fig.41. H1 results for the intercept of the pomeron trajectory from a fit to their reduced cross-section data

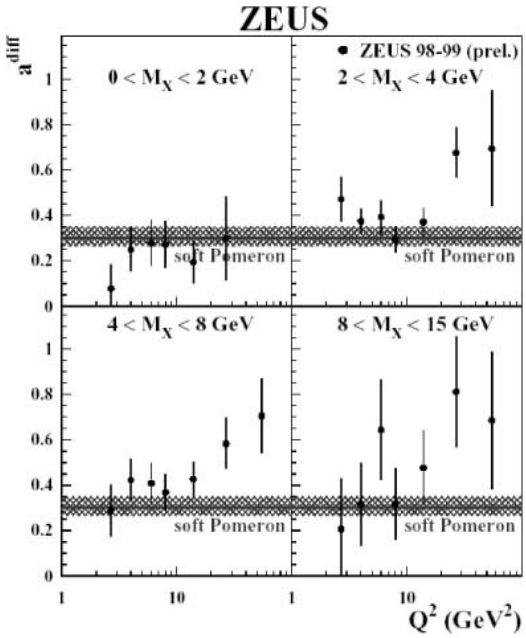

Fig.42. ZEUS results for the exponent of the W-dependence derived from a fit to the differential diffractive cross-section

The extracted exponent $a_{\rm diff}$ is plotted in Fig.42 as a function of Q^2 for several M_X-bins. Indicated are also the expected values for the exchange of a soft pomeron. For M_X-masses up to 2 GeV, $a^{\rm diff}$ is compatible with a soft pomeron exchange. For higher masses and for Q^2 above 10 GeV^2, the $a^{\rm diff}$-values deviate from the soft pomeron case.

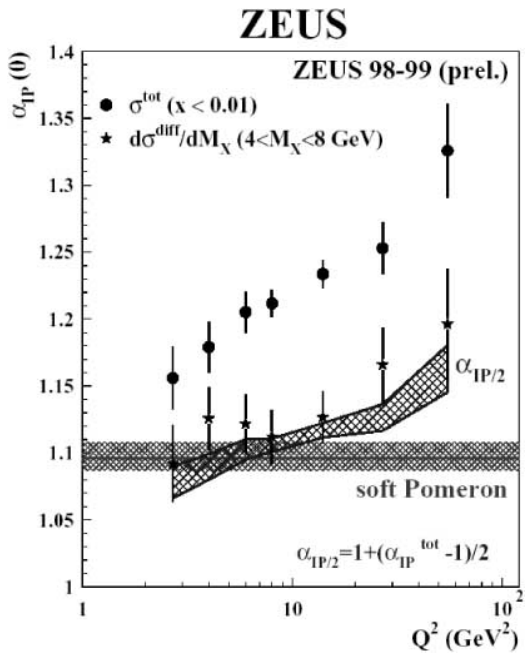

Fig.43. Intercepts of the pomeron trajectory from the differential diffractive cross-section and from the total DIS cross-section

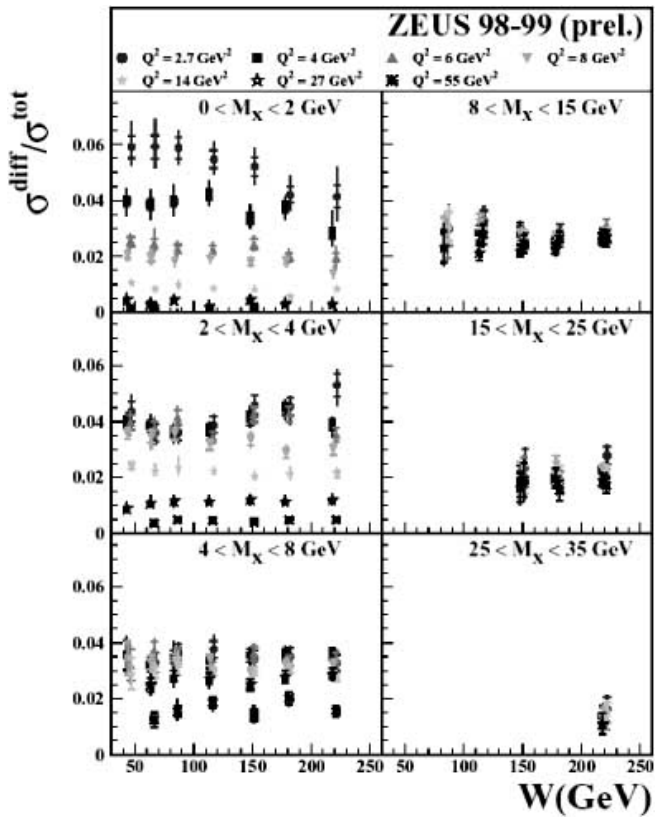

Fig.44. Intercepts of the pomeron trajectory from the differential diffractive cross-section and from the total DIS cross-section

5.4. Comparison of the Inclusive Diffractive with the Total DIS Cross-Section

The total $\gamma^* p$ cross-section is related to the imaginary part of the elastic forward scattering amplitude by the optical theorem. Therefore, $\sigma^{\rm tot}_{\gamma^* p} \propto (W^2)^{(\alpha^{\rm tot}_{I\!P}(0)-1)}$. The differential cross-section is proportional to the scattering amplitude squared. Therefore $\frac{d^2\sigma^{\rm diff}}{dm_X dt} \propto (W^2)^{2(\alpha^{\rm diff}_{I\!P}(0)-1)}$. Fig. 43 shows the $\alpha_{I\!P}(0)$ values extracted from ZEUS data corresponding to the total DIS cross-section (full points) and the diffractive differential cross-section (stars). Also shown are the soft pomeron expectation and a band which represents $1 + (\alpha^{\rm tot}_{I\!P}(0) - 1)/2$, including errors. It can be seen that the band coincides with the values of $\alpha^{\rm diff}_{I\!P}(0)$ which means

$$2(\alpha^{\rm diff}_{I\!P}(0) - 1) \approx (\alpha^{\rm tot}_{I\!P}(0) - 1)$$

and consequently

$$\frac{\frac{d^2\sigma^{\rm diff}}{dM_X dt}}{\sigma^{\rm tot}} \propto \frac{W^{2(\alpha^{\rm diff}_{I\!P}-1)}}{W^{(\alpha^{\rm tot}_{I\!P}-1)}} = {\rm const.}$$

This is in contradiction with the expectation from the optical theorem as outlined above. It is a similar situation as for the exclusive ρ production. The ratio of the total diffractive to the total DIS cross-section from the ZEUS data is plotted in Fig.44. The ratio has been obtained according to

$$r^{\rm diff}_{\rm tot} \equiv \frac{\sigma^{\rm diff}}{\sigma^{\rm tot}} = \frac{\int_{M_a}^{M_b} dM_X \frac{d\sigma^{\rm diff}_{\gamma^* p \to X}(M_Y < 2.3{\rm GeV})}{dM_X}}{\sigma_{\gamma^* p}} \; .$$

For $M_X < 2$ GeV, $r^{\rm diff}_{\rm tot}$ is falling with W whereas the ratio is constant for larger M_X like the ratio of the differential diffractive cross-section to the total cross-section. As a function of Q^2, $r^{\rm diff}_{\rm tot}$ is falling with Q^2 for low M_X. For $M_X > 8$ GeV, $r^{\rm diff}_{\rm tot}$ is constant with Q^2. This means it has the same Q^2-dependence as the total DIS cross-section and therefore the inclusive diffractive reaction is a leading twist process at high M_X.

5.5. H1 NLO QCD Fits to Diffractive Cross-Sections

The H1 Collaboration performed a NLO QCD fit to their diffractive cross-section data. They parametrized the diffractive parton distribution functions at $Q_0^2 = 3\,{\rm GeV}^2$ in the form

$$z p_i(z, Q^2) = \left[\sum_{j=1}^{n} C_j^i P_j(2z-1)\right]^2 e^{\frac{a}{z-1}}$$

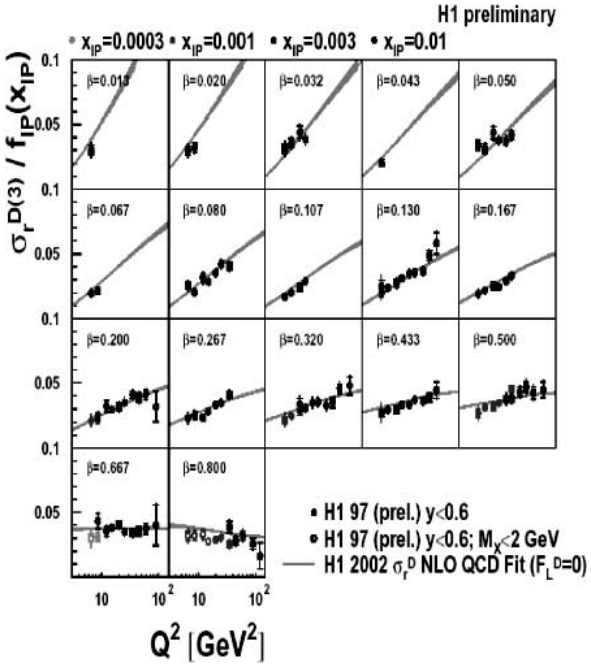

Fig.45. The reduced t-integrated diffractive cross-section devided by the pomeron flux plotted against Q^2 for different β-values from H1 data. The grey bands are results from a NLO QCD fit. For details, see the text

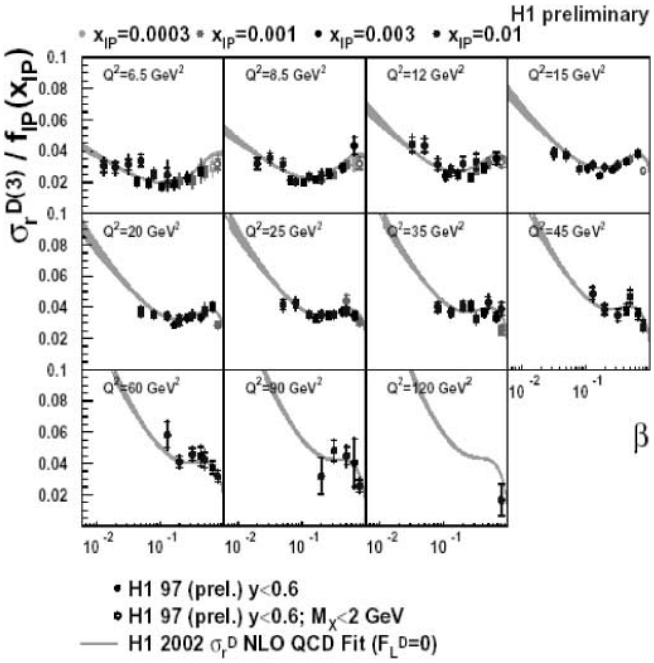

Fig.46. The same data as in fig.45 plotted against β for different Q^2-values together with the results of a NLO QCD fit. For details, see the text

with P_j being the Chebychev polynomial of order j. The fit result is compared to their data in Figs. 45 and 46. In Fig.45, the reduced cross-section, $\sigma_r^{D(3)}$, from H1 data integrated over t, the four-momentum transfer squared at the proton vertex, divided by the pomeron flux is shown as a function of Q^2 for different values of β. The fit describes the data well. In diffractive scattering, β plays the same role for the pomeron as Bjorken x for the proton in DIS. The observed variation of the Q^2-dependence of the reduced cross-section with β therefore indicates strong scaling violations. From the fit parameters, the H1 Collaboration concludes that the gluon content of the pomeron is $(75 \pm 15)\%$. In Fig.46, the reduced cross-section devided by the pomeron flux is shown as a function of β for different Q^2 values together with the fit results. Again the data are well described by the fit. Analogously to DIS, one sees a rise of the diffractive cross-section with decreasing β which gets stronger as Q^2 increases. The H1 NLO QCD fit is made under the assumption that all quark distribution functions are the same. One common singlet distribution and the gluon distribution are fitted. The singlet is given by

$$\sum(z) = u(z) + d(z) + s(z) + \overline{u}(z) + \overline{d}(z) + \overline{s}(z) \ .$$

Here, z is the momentum fraction of the parton entering the hard interaction. For lowest order pQCD, $z = \beta$ and $0 < \beta < z$ at higher orders. The singlet distribution and the gluon distribution from the NLO fit are shown in Fig.47 together with the experimental and theoretical error bands. In addition, a LO QCD fit has been performed. Its results are shown as a solid line.

5.6. Comparison of the ZEUS Results with the BEKW Model

The ZEUS Collaboration compared their data to the BEKW color dipole model [34]. In this model, the virtual photon splits into a quark-antiquark pair or a quark-antiquark-gluon state and interacts with the proton by the exchange of a two-gluon system which is color neutral. This is sketched in Fig.48.

The diffractive structure function receives two transverse contributions and one longitudinal contribution:

$$x_{I\!P} F_2^{D(3)} = c_T \cdot F_{q\overline{q}}^T + c_L \cdot F_{q\overline{q}}^L + c \cdot F_{gq\overline{q}}^T \ .$$

The three contributions in the BEKW model are parametrized as follows:

$$F_{q\overline{q}}^T = \left(\frac{x_0}{x_{I\!P}}\right)^{n_T(Q^2)} \beta(1-\beta),$$

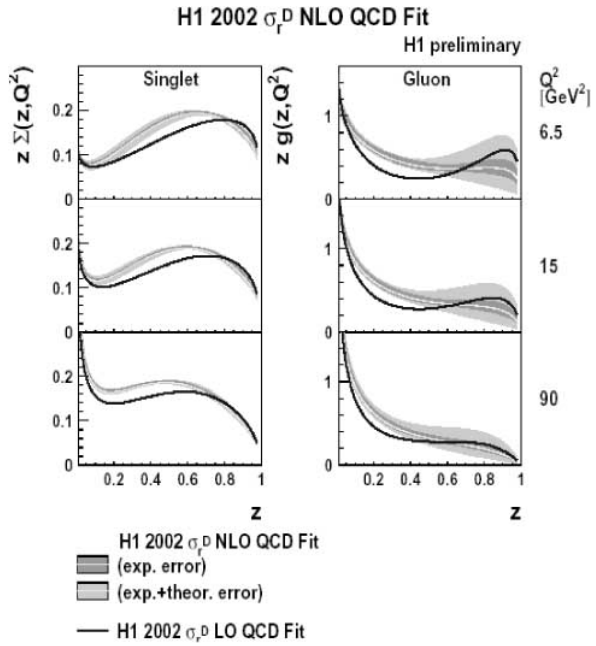

Fig.47. The diffractive singlet and gluon parton distributions from H1 QCD fits. For details see the text

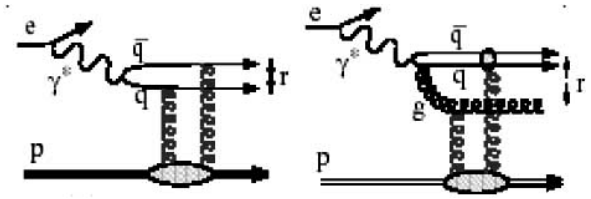

Fig.48. Picture of the BEKW color dipole model contributions

$$F_{q\overline{q}}^{L} = \left(\frac{x_0}{x_{I\!P}}\right)^{n_L(Q^2)} \frac{Q_0^2}{Q^2}\left[\ln(\frac{7}{4}+\frac{Q^2}{4\beta Q_0^2})\right]^2 \beta^3(1-\beta)^2,$$

$$F_{gq\overline{q}}^{T} = \left(\frac{x_0}{x_{I\!P}}\right)^{n_g(Q^2)} \ln(1+\frac{Q^2}{Q_0^2})(1-\beta)^{\gamma}.$$

The diffractive structure function, $F_2^{D(3)}$, integrated over t and multiplied by $x_{I\!P}$ from the the ZEUS data is shown in Fig.49 as a function of $x_{I\!P}$ for different Q^2 and β values. The well-known behavior is seen that the structure function rises with decreasing $x_{I\!P}$ and that the rise gets steeper with increasing Q^2. The data have been fitted by the BEKW color dipole.

A good fit to the ZEUS data has been achieved with $n_L(Q^2) = 0$, $N_T(Q^2) \approx n_G(Q^2) \approx n_1 \ln(\frac{Q^2}{Q_0^2})$ and the following parameters: $c_T = 0.118 \pm 0.027$, $c_L = 0.141 \pm 0.011$, $c_g = 0.0093 \pm 0.0003$, $n_1 = 0.068 \pm 0.0032$, $\gamma = 8.48 \pm 0.51$. The fit results in a small $(q\overline{q})_L$ contribution

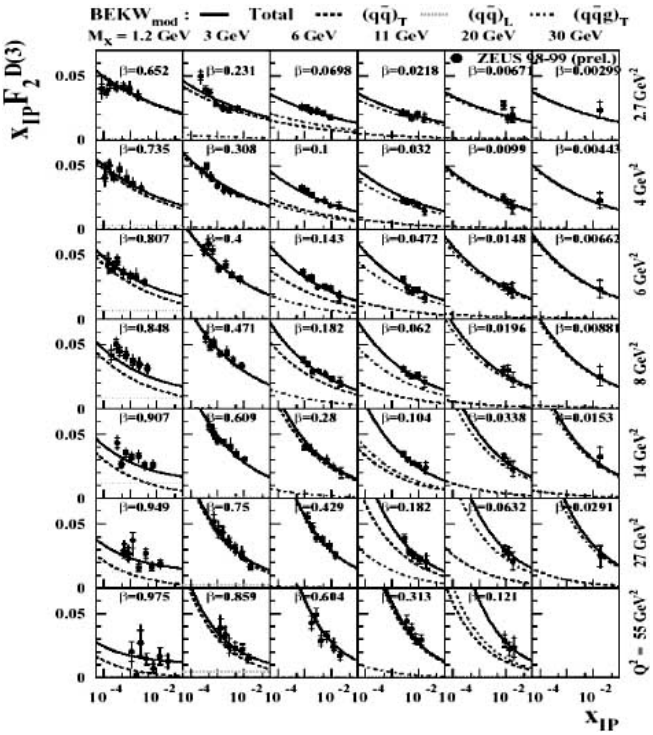

Fig.49. The t-integrated diffractive structure function from the ZEUS data. The lines are results from a BEKW color dipole fit

except at low M_X and high β. The $(gq\overline{q})_T$ contribution dominates at high M_X.

5.7. The Pomeron Structure Function

Using the Regge factorization theorem, one can define a pomeron structure function in the same way as the proton stucture function :

$$F_2^{D(3)}(Q^2, X_{I\!P}, \beta) = f_{I\!P/p}(Q^2, x_{I\!P}) F_2^{D(2)}(Q^2, \beta).$$

Here, $F_2^{D(2)}$ is the pomeron structure function. In the BEKW model, the flux factor is given by

$$f_{I\!P/p}(Q^2, x_{I\!P}) = \frac{C}{x_{I\!P}}\left(\frac{x_0}{x_{I\!P}}\right)^{n(Q^2)}.$$

The pomeron structure function, extracted from the ZEUS data at $x_{I\!P} = 0.01$, is shown in Fig.50 for several Q^2-values as a function of β.

The β-dependence of the pomeron structure function is similar to the x-dependence of the proton structure function. The pomeron structure function shows a local maximum at $\beta \approx 0.5$. At small β-values, it increases with decreasing β. The increase becomes steeper with higher Q^2.

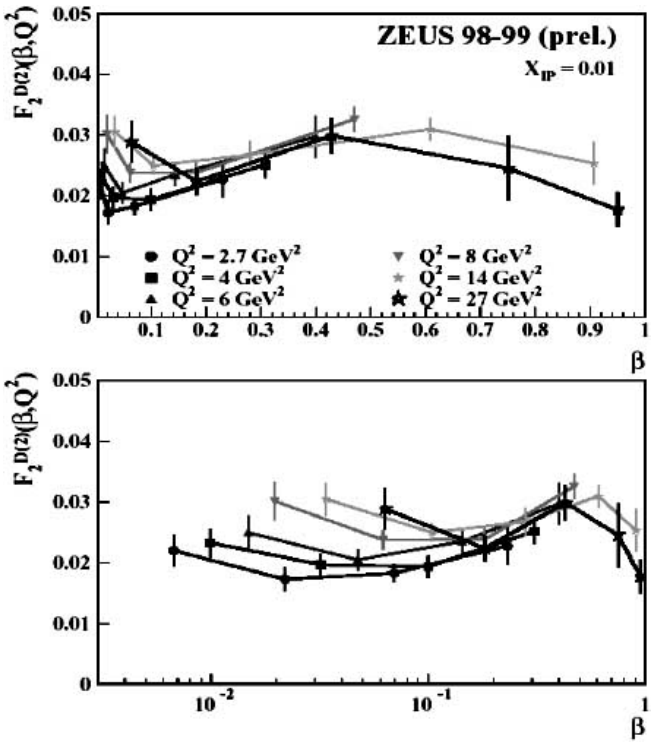

Fig.50. The pomeron structure function at $X_{IP} = 0.01$ from the ZEUS data as a function of β for several Q^2-values

6. Summary

Exclusive vector-meson production:

- Exclusive vector-meson production becomes a hard process when either the vector-meson mass is high (J/Ψ ...) or Q^2 or $|t|$ get large.
- In case of a hard process, the respective pomeron trajectory is not compatible with the soft pomeron one.
- The ratios of vector-meson production cross-sections do not agree with the pQCD predicted values but rather with the SU(4) expectations.
- The ratio of the exclusive ρ production to the total DIS cross-section is constant and does not rise with W as expected from the optical theorem. The ratio for the J/Ψ production, however, does rise.
- The ratio of the longitudinal to the transverse cross-section, σ_L/σ_T, rises with Q^2. At high Q^2, the longitudinal cross-section dominates.

Inclusive diffractive processes:

- Inclusive diffractive scattering becomes a hard process at high M_X and at high Q^2 and can be described by pQCD models. The diffractive parton distributions evolve with Q^2 according to DGLAP.
- The ratio of the inclusive diffractive cross-section to the total DIS cross-section is constant as a function of W and, for higher M_X, also as a function of Q^2. The latter indicates that hard diffractive scattering is a leading twist process.
- Strong scaling violations are present in hard diffractive scattering. The gluon content of the pomeron is about 75%.
- Color dipole models, like the BEKW one, can describe the inclusive diffractive data. The longitudinal dipole configuration contributes little. The $gq\overline{q}$ configuration dominates at high M_X.

1. *A Proposal* for a Large Electron-Proton Colliding Beam Facility at DESY, DESY HERA 81-10 (1981).
2. *Regge T.*// Nuov.Cim. **14** (1959) 951; **18** (1960) 947; *Collins P.* An Introduction to Regge Theory and High Energy Physics.— Cambridge University Press, Cambridge (1977).
3. *Chew G., Frautschi S.*// Phys.Rev.Lett. **7** (1961) 394; *Gribov N.*// Sov.Phys.JETP **14** (1962) 478; 395.
4. *Donnachi A., Landshoff P.V.*// Nucl.Phys. **B244** (1984) 322; Phys.Lett. **B296** (1992) 227.
5. *Lipatov L.N.*// Sov.J.Nucl.Phys. **23** (1976) 338; *Kuraev E.A., Lipatov L.N., Fadin V.S.*// Sov.Phys.JETP **45** (1977); *Balitsky Y.Y., Lipatov L.N.*// Sov.J.Nucl.Phys. **28** (1978) 822.
6. *Sakurai J.J.* "Currents and Mesons".— University of Chicago Press, Chicago (1969); *Fraas H., Schildknecht D.*// Nucl.Phys. **B14** (1969) 543.
7. *Berger C. et al.*// Phys. Lett. **39B** (1972) 659; *SWT Collab., Eisenberg Y. et al.*// Phys. Rev. **D5** (1972) 15; *Park J. et al.*// Nucl. Phys. **B36** (1972) 404; *SBT Collab., Ballam J. et al.*// Phys. Rev. **D5** (1972) 545; *SBT Collab, Ballam J. et al.*//Ibid. **D7** (1973) 3150; *Gladding G.E. et al.*//Ibid. **D8** (1973) 3721; *Struczinski W. et al.*// Nucl. Phys. **B108** (1976) 45; *Egloff R.M. et al.*// Phys. Rev. Lett. **43** (1979) 657; *OMEGA Photon Collab., Aston D. et al.*// Nucl. Phys. **B209** (1982) 56; *H1 Collab., Aid S. et al.*// Ibid. **B463** (1996) 3; *ZEUS Collab., Breitweg J. et al.*// Eur.Phys.J. **C2** (1998) 247.
8. *Crouch H.R. et al.*// Phys. Rev. **155** (1967) 1468; *ABBHHM Collab., Erbe R. et al.*// Ibid. **175** (1968) 1669; *Davier M. et al.*// Phys. Rev. **D1** (1970) 790; *SWT Collab., Eisenberg Y. et al.*// Ibid. **D5** (1972) 15; *SBT Collab., Ballam J. et al.*// Ibid. **D7** (1973) 3150; *Struczinski W. et al.*// Nucl. Phys. **B108** (1976) 45; *Egloff R.M. et al.*// Phys. Rev. Lett. **43** (1979) 1545 and **44** (1980) 690 (Erratum); *Breakstone A.M. et al.*// Phys. Rev. Lett. **47** (1981) 1782; *Aston D. et al.*// Nucl. Phys. **B209** (1982) 56; *LAMP2 Group, Barber D.P. et al.*// Z. Phys. **C26** (1984) 343; *OMEGA Collab., Atkinson M. et al.*// Nucl. Phys. **B231** (1984) 15; *Busenitz J. et al.*// Phys. Rev. **D40** (1989) 1.

9. *Busenitz J. et al.*// Phys. Rev. **D40** (1989) 1; *Erbe R. et al.*// Phys. Rev. **175** (1968) 1669; *Berger C. et al.*// Phys. Lett. **B39** (1972) 659; *Ballam J. et al.*// Phys. Rev. **D7** (1973) 3150; *Besch H.J. et al.*// Nucl. Phys. **B70** (1974) 257; *Behrend H.J. et al.*// Phys. Lett. **B56** (1975) 408; *Barber D.P. et al.*// Ibid. **B79** (1978) 150; *Aston D. et al.*// Nucl. Phys. **B172** (1980) 1; *Atkinson M. et al.*// Z. Phys. **C27** (1985) 233; *ZEUS Collab., Derrick M. et al.*// Phys.Lett. **B73** (1996) 259.

10. *Knapp B. et al.*// Phys. Rev. Lett. **34** (1975) 1040; *Camerini U. et al.*// Ibid. **35** (1975) 483; *Gittelman B. et al.*// Ibid. 1616; *Nash T. et al.*// Ibid. **36** (1976) 1233; *BFP Collab., Clark A.R. et al.*// Ibid. **43** (1979) 187; *EMC Collab., Aubert J.J. et al.*// Nucl. Phys. **B213** (1983) 1; *NA14 Collab., Barate R. et al.*// Z. Phys. **C33** (1987) 505; *E687 Collab., Frabetti P.L. et al.*// Phys. Lett. **B316** (1993) 197; *NMC Collab., Arneodo M. et al.*// Ibid. **B332** (1994) 195; *E401 Collab., Binkley M. et. al.*// Phys Rev. Lett. **48** (1982) 73; *E516 Collab., Denby B.H. et al.*// Ibid. **52** (1984) 795; *ZEUS Collab., Breitweg J. et al.*// Z.Phys. **C75** (1997) 215; *ZEUS Collab., Chekanov S. et al.*// Eur.Phys.J. **C24** (2002) 345; *H1 Collab., Adloff C. et al.*// Phys.Lett. **B483** (2000) 23; *H1 Collab., Adloff C. et al.* Contribution to DIS 2003.— St.Petersburg, Russia.

11. *H1 Collab., Adloff C. et al.*// Phys.Lett. **B541** (2002) 251; *ZEUS Collab.*// Contribution to Intern. Europhysics Conf. on High Energy Physics, July 2001, Budapest, Hungary.

12. *H1 Collab., Adloff C. et al.*// Phys.Lett. **B483** (2000) 23; *ZEUS Collab., Breitweg J. et al.*//Ibid. **B437** (1998) 432.

13. *Frankfurt L., McDermott M., Strikman M.*// J. High Energy Phys. **103** (2001) 45; *CTEQ Collab., Lai H.L. et al.*// Eur.Phys.J. **C12** (2000) 375; *Martin A.D. et al.*// Ibid. **C4** (1998) 463.

14. *H1 Collab., Adloff C. et al.*// Eur.Phys.J. **C13** (2000) 371; *H1 Collab., Aid S. et al.*// Nucl.Phys. **B468** (1996) 3; *Zeus Collab.*// Contributed Paper 594 to European Phys. Soc. Conf., 2001, Budapest, Hungary; *ZEUS Collab., Breitweg J. et al.*// Eur.Phys.J. **C6** (1999) 603.

15. *ZEUS Collab.*// Contributed Paper 813 to ICHEP 2002, Amsterdam, The Netherlands; *ZEUS Collab., Breitweg J. et al.*// Eur.Phys.J. **C6** (1999) 603; *H1 Collab., Aid S. et al.*// Nucl.Phys. **B468** (1996) 3.

16. *Martin A.D., Ryskin M.G., Teubner T.*// Phys.Rev. **D62** (2000) 14022; *CTEQ Collab., Lai H.L. et al.*// Eur.Phys.J. **C12** (2000) 375.

17. *Frankfurt L., Koepf W., Strikman M.*// Phys.Rev. **D57** (1998) 512.

18. *Bartels J. et al.*// Phys.Lett. **B375** (1996) 301.

19. *Ivanav D.Yu.*// Ibid. **B478** (2000) 101; *Ivanav D.Yu.*// Phys.Rev. **D53** (1996) 3564.

20. *Gribov V., Lipatov L.*// Sov.J.Nucl.Phys. **15** (1972) 438 and 675; *Dokshitzer Y.*// Sov.Phys. JETP **46** (1977) 641; *Altarelli G., Parisi G.*// Nucl.Phys. **B126** (1977) 298.

21. *Martynov E., Predazzi E., Produkin A.*// Phys.Rev. **D67** (2003) 74023; *Martynov E., Predazzi E., Produkin A.*// Eur.Phys.J. **C26** (2002) 271.

22. *Brodsky J. et al.*// Phys.Rev. **D50** (1994) 3134.

23. *Schilling K., Wolf G.*// Nucl.Phys. **B61** (1973) 381.

24. *Martin A.D., Ryskin M.G., Teubner T.*// Phys.Rev. **D62** (2000) 14022; *Martin A.D., Ryskin M.G., Teubner T.*// Ibid. **D56** (1997) 3007; *Martin A.D., Ryskin M.G., Teubner T.*// Ibid. **D55** (1997) 4329.

25. *Wieczorek E., Matveev V.A., Robaschik D.*// Theor.Mat.Phys. **19** (1974) 315; *Bartels J., Loewe M.*// Z.Phys. **C12** (1982) 263; *Ji X.*// Phys.Rev. **D58** (1997) 7114; *Radyushkin A.V.*// Ibid. **D58** (1998) 114008.

26. *Frankfurt L.L., Freund A., Strikman M.*// Ibid. 114001; Erratum // Ibid. **D59** (1999) 119901; *Ji X.*// Phys.Lett. **B78** (1997) 610; *Golec-Biernat K., Martin A.*// Phys.Rev. **D59** (1999) 14029.

27. *ZEUS Collb., Chekanov S. et al.*// DESY-03-59, hep-ex/0305028, submitted to Phys.Lett.B.

28. *Ingelman G., Schlein P.*// Phys.Lett. **B152** (1985) 256.

29. *Feynman R.P.* Photon-Hadron-Interactions.— Benjamin, New.York. (1972), lectures 50-54.

30. *Zeus Collab., Derrick M. et al.*// Z.Phys. **C70** (1996) 391; *Zeus Collb., Breitweg J. et al.*// Europ.Phys.J. **C6** (1999) 43.

31. *Collins J.*// Phys.Rev. **D57** (1998) 3051 and erratum-ibid. **D62** (2000) 19902.

32. *H1 Collab., Adloff C. et al.*// Z.Phys. **C76** (1997) 613; *H1 Collab.*// Contributed papers 980 and 981 to ICHEP 2002, Amsterdam, The Netherlands.

33. *ZEUS Collab., Breitweg J. et al.*// Europ.Phys.J. **C6** (1999) 43.

34. *Bartels J., Ellis J., Kowalski H., Wuesthoff M.*// Ibid. **C7** (1999) 443.

ДИФРАКЦІЯ В ГЛИБОКО НЕПРУЖНОМУ РОЗСІЯННІ НА ПРИСКОРЮВАЧІ HERA

Б. Лор

Р е з ю м е

Наведено результати експериментів колаборацій H1 і ZEUS з дифракційних реакцій в фотонародженні та глибоко непружному розсіянні, одержані на прискорювачі HERA. Описано дані з ексклюзивного народження векторних мезонів, інклюзивного дифракційного розсіяння, а також з глибоко віртуального комптонівського розсіяння (ГВКР). Ці дані порівнюються з редже-феноменологією; і для різних реакцій, за винятком ГВКР, одержуються траєкторії Померанчука. Порівнюються також з експериментальними даними підгонки і передбачення пертурбативної КХД. З опису даних в цих двох підходах показано, що відбувається перехід від м'якої дифракції до жорсткої у випадку, коли маса дифракційно народжуваної системи стає більшою, або від'ємний квадрат переданого чотиріімпульсу Q^2 від електрона/позитрона до дифракційно народжуваної системи чи абсолютна величина квадрата переданого чотиріімпульсу $|t|$ від протона до дифракційно народжуваної системи стають більшими.

ДИФРАКЦИЯ В ГЛУБОКО НЕУПРУГОМ РАССЕЯНИИ НА УСКОРИТЕЛЕ HERA

Б. Лор

Р е з ю м е

Представлены результаты экспериментов коллабораций H1 и ZEUS по дифракционным реакциям в фоторождении и глубоко неупругом рассеянии, полученные на ускорителе HERA. Описаны данные по эксклюзивному рождению векторных мезонов, инклюзивному дифракционному рассеянию, а также по глубоко виртуальному комптоновскому рассеянию (ГВКР). Эти данные сравниваются с редже-феноменологией; и для различных реакций, за исключением ГВКР, извлекаются траектории Померанчука. Сравниваются также с экспериментальными данными подгонки и предсказания пертурбативной КХД. Из описания данных в этих двух подходах показано, что происходит переход от мягкой дифракции к жесткой в случае, когда масса дифракционно рождаемой системы становится больше, либо отрицательный квадрат переданного четыреимпульса Q^2 от электрона/позитрона к дифрационно рождаемой системе или абсолютная величина квадрата переданного четыреимпульса $\mid t \mid$ от протона к дифрационно рождаемой системе становятся большими.